


## Reactive wetting of metallic/ceramic ( $\text{Al}/\alpha\text{-Al}_2\text{O}_3$ ) systems: a parallel molecular dynamics simulation study

Gürcan ARAL\*

Department of Physics, Faculty of Science, İzmir Institute of Technology, İzmir, Turkey

Received: 30.05.2019

Accepted/Published Online: 18.11.2019

Final Version: 12.02.2020

**Abstract:** The reactive wetting process of a flat solid alumina ( $\alpha\text{-Al}_2\text{O}_3$ ) ceramic surface by metallic aluminum (Al) nanodroplets with different shapes (spherical, cylindrical, and layer) is studied using parallel molecular dynamics (MD) simulations based on a variable charge MD method, with focuses on heat transfer, mass transfer, and the structure of the reactive region at the  $\text{Al}/\alpha\text{-Al}_2\text{O}_3$  interface. We find that the diffusion of oxygen (O) atoms from the substrate into the droplet leads to the formation of a continuous layer of reaction product at the interface. The diffusion length of oxygen atoms into the spherical Al droplet is found to be  $\sim 7.3$  Å, and the number density of O atoms at the  $\sim 5$  top layers of the substrate decreases substantially. As a result, the structural correlations near the reactive region differ considerably from those in the solid substrate. Heat generated by the exothermic reactions in the reactive region is transferred to both the substrate and the droplet. The heat transfer is found to be sensitive to droplet shape.

**Key words:** Variable charge method, molecular dynamics simulations, wetting, alumina, aluminum

### 1. Introduction

Wetting of ceramic substrates by liquid metals is important for various applications such as coating, joining, and composite processing. In metal-ceramic systems, the wetting process is governed by interfacial energies [1–8], which depend strongly on chemical reactions at the metal/ceramic interfaces [2–4,6,9–14]. The wettability kinetics, behaviors, and properties in reactive  $\text{Al}/\alpha\text{-Al}_2\text{O}_3$  systems are highly sensitive to the experimental testing procedure, conditions, and temperature [9–12]. The presence of thick and continuous oxide shell layers on Al droplets prevents true contact with the ceramic materials, which hinders eventual ion diffusion at the metallic/ceramic interface, consequently leading to poor wetting (i.e. large contact angles values) and spreading on the  $\alpha\text{-Al}_2\text{O}_3$  substrate [10,12,13]. The nonwetting to wetting transition occurs in Al/ceramic systems at approximately above  $T = 1273$  K (critical temperature), which corresponds to the melting temperature of the preexisting amorphous oxide shell layer on the free surface of the Al droplet [12].

During the wetting of an alumina ( $\alpha\text{-Al}_2\text{O}_3$ ) substrate by a liquid aluminum (Al) droplet, for example, the interfacial energy acts as a driving force for the diffusion of oxygen atoms from the  $\alpha\text{-Al}_2\text{O}_3$  substrate into the liquid Al, through which the interfacial energy is lowered [3,4,6,9,15]. Wettability and nonwettability are characterized by the wetting contact angle  $\theta$  for the liquid droplet on the solid substrate that characterizes the bonding properties of the metallic droplet/ceramic substrate. Young's equation [16–19] states that

$$\theta = \text{Cos}^{-1}[(\gamma_{SV} - \gamma_{LS})/\gamma_{LV}], \quad (1)$$

\*Correspondence: gurcanaral@iyte.edu.tr

where  $\gamma_{SV}$ ,  $\gamma_{LS}$ , and  $\gamma_{LV}$  are the solid/vapor, liquid/solid, and liquid/vapor interfacial energies. Contact-angle measurements using a sessile drop technique have been used extensively to study thermodynamics and kinetics of wetting as a function of temperature, alloying elements, and environment (e.g., oxygen partial pressure). The effect of temperature on the wettability of an  $\text{Al}_2\text{O}_3$  single crystal by metallic Al was investigated at 933–1273 K by Laurent et al. [18]. They found that the contact angle was a linearly decreasing function of temperature. Contact angles also change with time during wetting. Levi et al. systematically studied the investigated reactive wetting process of a metallic liquid Al droplet on a solid sapphire substrate and time evaluation of the wetting contact angle [15] by using the sessile drop technique. The contact angle was found to decrease with time at constant temperature and approached an asymptotic value, called the apparent true contact angle, which is  $\sim 90^\circ$  at 900 K.

Oxygen atoms in  $\alpha\text{-Al}_2\text{O}_3$  dissolve into liquid Al to form partially ionic Al-O bonds, due to the strong affinity of aluminum to oxygen [7]. This bonding results from charge transfer between Al and O atoms [2,8,20]. The resulting formation of a solder joint layer (or continuous oxygen-rich layer) explains the strong adhesion of the Al/ $\alpha\text{-Al}_2\text{O}_3$  interface because of the strong ionic bonding [7,15,21] and it may significantly modify the chemical and physical properties [22] of the metal/ceramic interface.

In the present work, we use molecular dynamics (MD) simulations on parallel computers to study the atomistic mechanisms of reactive wetting of a flat  $\alpha\text{-Al}_2\text{O}_3$  substrate by an Al nanodroplet, with focuses on heat and mass transfer, temporal change of the contact angle, effects of droplet shape (spherical, cylindrical, and layer), and structural correlations in the reactive region. The variable-charge MD scheme is employed to properly take into account the charge transfer and chemical reaction between Al and O atoms. The organization of the paper is as follows: Section 2 describes the simulation method and schedule, and results are given in Section 3. Finally, Section 4 contains the conclusions.

## 2. Interatomic potential model and simulation schedule

In classical MD simulations, the simulating of a physical system is represented completely by a set of  $N$  atoms or molecules. The subsequent time evolution of the trajectories, i.e. positions,  $\{\mathbf{r}_i \mid i = 1, \dots, N\}$ , and velocities,  $\{\mathbf{v}_i \mid i = 1, \dots, N\}$ , for each individual atom is followed mainly by numerically integrating Newton's equations of motion:

$$m_i \frac{d^2 \mathbf{r}_i}{dt^2} = \mathbf{F}_i, \quad (2)$$

where  $m_i$  is the mass of atom  $i$  and the force acting on the  $i$ th atom is derived from the partial derivative of total potential energy as

$$\mathbf{F}_i = - \frac{\partial V}{\partial \mathbf{r}_i}. \quad (3)$$

The interaction of the interatomic potential energy (i.e. potential) function,  $V$ , of the atoms is the most essential input element of MD simulations. An analytical functional form of interatomic potential principally describes all interactions between atoms in a given system. The MD simulation method is based on the numerical integration of Equation (2) using a discrete time step  $\Delta t$ , given  $6N$  initial conditions,  $\{\mathbf{r}_i(t = 0), \mathbf{v}_i(t = 0)\}$ . We use the highly reliable and realistic interatomic potential scheme called the ES+ model, based on the variable-charge method [23]. In this scheme, atomic charges,  $\{q_i \mid i = 1, \dots, N\}$ , are determined dynamically, reflecting changes of their local environment [24,25]. The ES+ model thus enables the description of chemical

reactions such as metallic and ionic bond formation and breakage at the Al/ $\alpha$ -Al<sub>2</sub>O<sub>3</sub> interface. The ES+ model has been applied successfully to simulations of a wide range of physical properties involving Al and Al<sub>2</sub>O<sub>3</sub>, such as the oxidation of Al nanoparticles [23,26].

The total interatomic potential energy,  $V$ , in the ES+ model is a sum of electrostatic ( $V_{ES}$ ) and embedded-atom ( $V_{EAM}$ ) terms:  $V(\{\mathbf{r}_i, q_i\}) = V_{ES}(\{\mathbf{r}_i, q_i\}) + V_{EAM}(\{\mathbf{r}_i\})$ . The total electrostatic energy in turn consists of local atomic ( $V_i(q_i)$ ) and electrostatic ( $V_{ij}(\mathbf{r}_{ij}; q_i, q_j)$ ) energies:

$$V_{ES} = \sum_i V_i(q_i) + \frac{1}{2} \sum_{i \neq j} V_{ij}(\mathbf{r}_{ij}; q_i, q_j), \quad (4)$$

where  $\mathbf{r}_{ij} = \mathbf{r}_i - \mathbf{r}_j$  and

$$V_i(q_i) = V_i(0) + \chi_i q_i + \frac{1}{2} J_i q_i^2, \quad (5)$$

$$V_{ij}(\mathbf{r}_{ij}; q_i, q_j) = \int d^3 \mathbf{r}_1 \int d^3 \mathbf{r}_2 \frac{\rho_i(\mathbf{r}_1, q_i) \rho_j(\mathbf{r}_2, q_j)}{r_{12}}. \quad (6)$$

In Equation (5), the self-energy,  $V_i(q_i)$ , of atom  $i$  is expressed as a second-order Taylor expansion in terms of the partial atomic charge,  $q_i$ , where  $\chi_i$  and  $J_i$  are the electronegativity [27] and hardness (self-Coulomb repulsion) [28] of atom  $i$ , respectively.

The electrostatic pair energy in Equation (6) depends on the atomic valance charge distributions (including the nuclear point charge),  $\rho_i(\mathbf{r}_i; q_i)$ , which take an extended form of a Slater-type 1s atomic orbital:

$$\rho_i(\mathbf{r}; q_i) = Z_i \delta(\mathbf{r} - \mathbf{r}_i) + (q_i + Z_i) \left(\frac{\zeta_i}{\pi}\right) \exp(-2\zeta_i |\mathbf{r} - \mathbf{r}_i|), \quad (7)$$

where  $\zeta_i$  is the decay length for the atomic orbital and  $Z_i$  is the effective point core charge.

The temporal evolution of atomic charges  $\{q_i\}$  is evaluated at every MD step, so as to minimize the electrostatic energy  $V_{ES}$  with the electro-neutrality principle,  $\sum_i q_i = 0$ . The determination of the atomic charges at every MD step involves the solution of a dense linear system of equations and hence requires  $O(N^3)$  operations. A spatial decomposition approach is used to implement the variable-charge MD algorithm on parallel computers [29].

The initial MD configuration for the reactive wetting simulation is schematically shown in Figure 1. The flat solid alumina ( $\alpha$ -Al<sub>2</sub>O<sub>3</sub>) ceramic slab containing 20,160 atoms has dimensions of 5.69 (length) nm, 5.75 (width) nm, and 5.21 (height) nm in the x, y, and z directions, respectively, where the z-axis is parallel to [0001]. In addition, a spherical metallic Al nanodroplet with a diameter of 2.3 nm is located in position of 0.14 nm above the top surface of the flat solid alumina ceramic slab. (The crystalline structure of  $\alpha$ -Al<sub>2</sub>O<sub>3</sub> solid ceramic forms of close-packed planes of O ions is arranged in the order of ABAB...; these planes are perpendicular to the [0001] direction, with Al ions filling up two-thirds of the octahedrally organized positions between the O layers. The coordination numbers of the Al and O atoms are 6 and 4, respectively [30].) The top surface of the  $\alpha$ -Al<sub>2</sub>O<sub>3</sub> (0001) slab is chosen such that it is terminated with a layer of close-packed O ions. The bottom of the ceramic slab is put in a position at  $z = 0.82$  nm in the simulation box of heights 0.90 nm (spherical), 0.80 nm (cylindrical), and 0.84 nm (layer) for metallic Al droplet cases in the z-direction, to build free surfaces both at the top and the bottom. Periodic boundary conditions (PBCs) are employed in all Cartesian directions except

along the z-directions, and hard walls are placed at the top and bottom in the z-direction of the simulation MD box to keep the atoms inside. The atomic charges of the  $\alpha$ - $\text{Al}_2\text{O}_3$  substrate in the region of  $z < 4.0$  nm are fixed at constant values corresponding to the bulk solid  $\alpha$ - $\text{Al}_2\text{O}_3$  crystal.

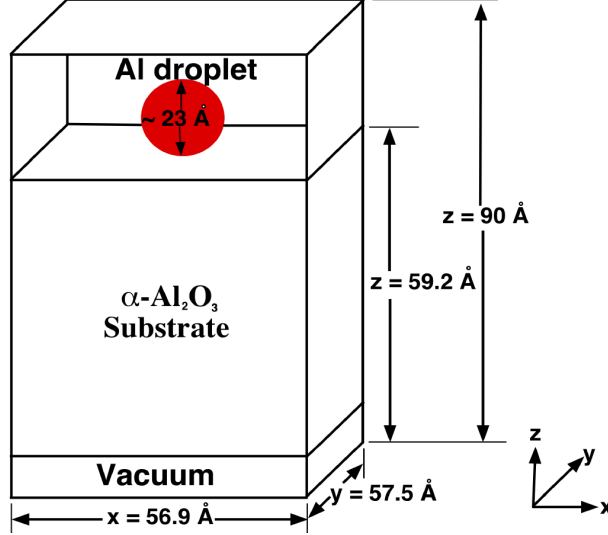


**Figure 1.** Schematic view of the initial simulated system configuration with PBCs employed in the x- and y-directions during the reactive wetting process.

The solid  $\alpha$ - $\text{Al}_2\text{O}_3$  ceramic slab is initially thermalized for 2000 time steps (the unit time step is  $\Delta t = 1$  fs) as follows: If the kinetic energy (KE) of an atom exceeds 200 K, it is reduced by a factor of 0.5, while the atomic temporal charges are relaxed at every MD time step. During the subsequent 2500 steps, the total average KE of the simulating system is reduced to 0 K and the temporal atomic charges are determined at every 10th MD step.

Wetting simulations are implemented by putting either i) a spherical metallic droplet of diameter 2.3 nm containing 551 Al atoms, ii) a cylindrical metallic Al droplet of diameter 1.56 nm containing 706 Al atoms, or iii) a layer metallic Al slab of height 1.55 nm along the z-direction containing 3,069 Al atoms in a position of 0.14 nm above the top surface of the solid ceramic slab surface. The velocity-Verlet algorithm method of integrating Newton's equations of motion [31], in Equation (2), is used with the unit MD time step  $\Delta t = 1$  fs. The microcanonical ensemble [32] is used, in which the total energy of the system is maintained to more than 1 part in  $10^2$  over the whole simulation of 8.5 ps. New temporal atomic charges are determined numerically at each time step by using the electronegativity equalization method, which is equivalent to minimizing the electrostatic energy.

### 3. Results and discussion

#### 3.1. Results on a spherical nanodroplet

We use the variable-charge MD method to study heat transfer on the atomic scale during the wetting of the flat  $\alpha$ - $\text{Al}_2\text{O}_3$  surface by the spherical Al droplet. Figure 2 indicates the time evolution of the metallic droplet shape as well as the temperature distribution in the metallic droplet and ceramic substrate at different times during our MD simulation of the reactive wetting process. When put down on the surface of the flat ceramic substrate, the metallic droplet starts to wet the ceramic substrate. The chemical reactions during the reactive wetting of

Al/ $\alpha$ -Al<sub>2</sub>O<sub>3</sub> are highly exothermic and thus can be seen as rapid increases in temperature. Quick chemical reactions taking place at the beginning step of the simulation are shown in Figure 2. The initial reaction site is near the contact point between the Al droplet and the flat  $\alpha$ -Al<sub>2</sub>O<sub>3</sub> substrate, and its extension can be managed by the diffusion of both Al and O atoms. These chemical reactions initially produce an intense heat flow through the contact region, which propagates into both sides of the interface. Around the contact region between the droplet and substrate, the temperature is relatively high, causing the metallic Al droplet to melt as well as oxidize it. Consequently, the metallic droplet spreads over the substrate and changes its shape to form a hemispherical cap (see Figure 2).

Dynamic charge transfer between Al and O atoms, associated with the dissolution of the  $\alpha$ -Al<sub>2</sub>O<sub>3</sub> ceramic into the Al droplet, leads to ionic interactions between dissolved O atoms and Al-droplet atoms in the developing solder joint layer. As a result of the chemical reaction between Al and O atoms across the interface and the formation of the continuous oxide layer with ionic bonding, noticeable atomic charge transfer between Al and O atoms in this reactive region is observed in Figure 3. The magnitudes of the effective valance charges of oxygen atoms are reduced from the bulk  $\alpha$ -Al<sub>2</sub>O<sub>3</sub> value at the interface between the two materials (see Figure 3).

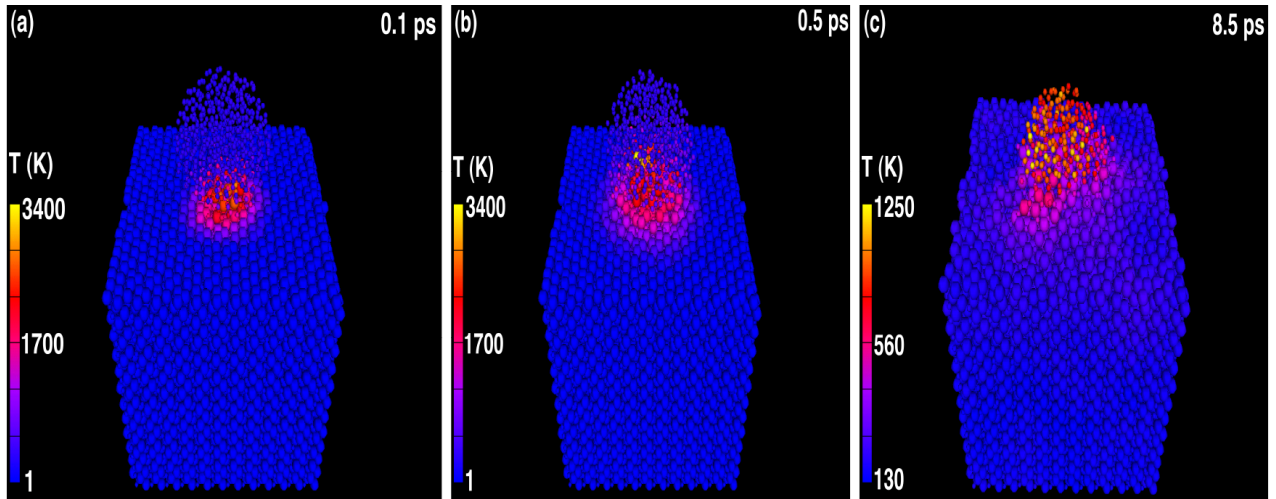


**Figure 2.** Snapshots from a reactive wetting simulation showing the temperature distribution at times of (a) 0.1 ps, (b) 0.5 ps, and (c) 8.5 ps. O and Al atoms are shown by larger and smaller spheres, respectively, and are colored by the temperature of the atoms.

Mechanisms of heat transfer from the droplet/substrate contact to the  $\alpha$ -Al<sub>2</sub>O<sub>3</sub> substrate and the Al droplet are investigated using temperature profiles along the z-direction. Figure 4 shows the time evolution of the temperature profile, calculated using bins of thickness of 4 Å. The initial configuration of the ceramic substrate ( $z = 0.827$ – $5.926$  nm) and the spherical metallic Al droplet ( $z = 6.067$ – $8.438$  nm) along the z-direction are shown as vertical lines in Figure 4, where the reactive interface is initially located at a z value of  $\sim 6.1$  nm. Initially, both the metallic droplet and the ceramic substrate are at  $T = 0$  K. As the metallic droplet begins to wet the substrate, very rapid chemical reactions generate heat, as seen in the temperature increase at the interface (see the sharp peak in the temperature profile at 1 ps around  $z = 6.1$  nm in Figure 4). The subsequent decrease in temperature is due to the reduction in the chemical reaction rate and the heat transfer from the

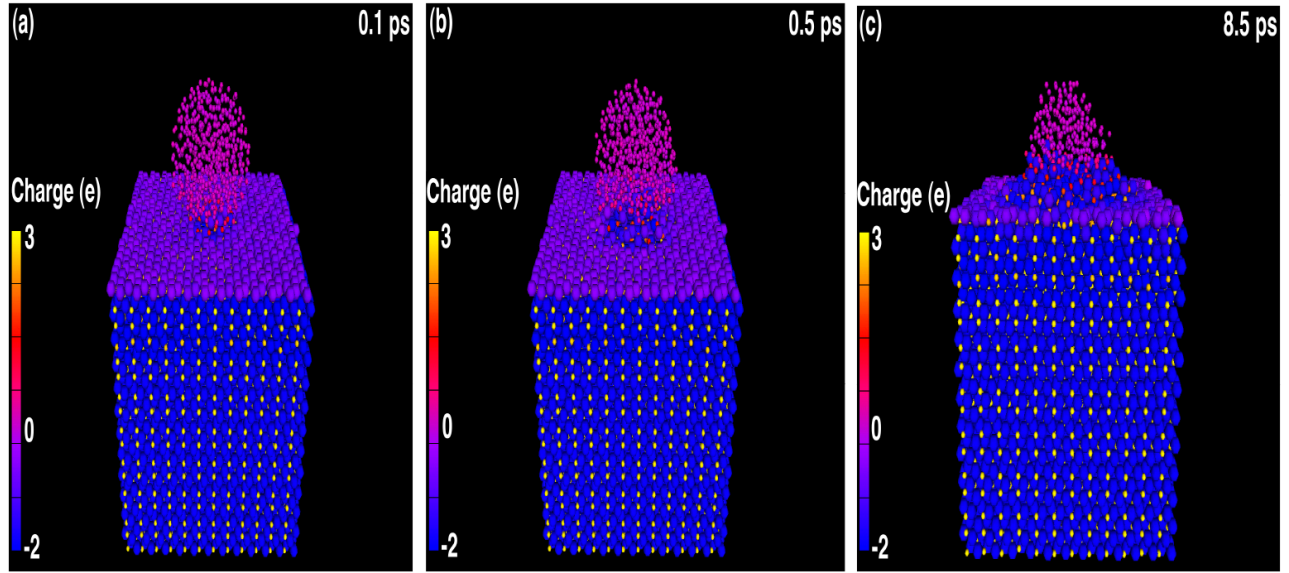


**Figure 3.** Time evolution of the temporal atomic charges and their redistributions in the wetting process taken at (a) 0.1 ps, (b) 0.5 ps, and (c) 8.5 ps for the spherical droplet. O and Al atoms are shown by larger and smaller spheres, respectively, and are colored by the sign as well as magnitude of charges.

reactive region to the droplet/substrate. The temperature is higher within the metallic droplet as compared to the ceramic substrate. This is understandable because the heat transfer is more rapid in the metallic droplet than in the ceramic substrate, as the thermal conductivity of Al (237 W/mK) is higher than that of alumina (40 W/mK) at 300 K [30]. At 3 ps, the metallic Al droplet is in the molten state because the temperature of the droplet is higher than the melting temperature of Al (933 K). The heat transfer thus results in a solid-to-liquid phase transformation in the metallic Al droplet. Figure 4 shows that, when the Al droplet is placed on the  $\alpha$ -Al<sub>2</sub>O<sub>3</sub> at 0 K, highly exothermic reactions take place at the interface. This is followed by rapid initial heat transfer from the chemically reactive region to the droplet/substrate, which eventually subsides. This is reminiscent of calorimetric experimental results, where rapid heat evolution within 5–10 min is followed by slow evolution of the heat flow for several hours [33].

Next we study the penetration of O atoms from the ceramic substrate into the metallic droplet and the resulting formation of a continuous O-rich layer as a reaction product in the reactive region. Figure 5 shows the temperature distribution of O atoms (Al atoms are removed for clear presentation) at times of 0.5 and 5.5 ps. Some O atoms from the  $\alpha$ -Al<sub>2</sub>O<sub>3</sub> substrate in the vicinity of the droplet/ceramic substrate initially diffuse rapidly into the Al droplet, partially oxidizing the Al droplet and causing the adhesion of the Al droplet to the substrate in the reactive surface region near the physical contact between the droplet and the substrate. Namely, the initialization of chemical reaction in the wetting process provides an additional driving force for the diffusion of dissolved O ions from the  $\alpha$ -Al<sub>2</sub>O<sub>3</sub> ceramic slab to the Al droplet, and this leads to adhesion of the metallic Al droplet to the ceramic substrate through formation of Al-O bonds. The solid substrate acts obviously as a source of O atoms donor (dissolution of O from the  $\alpha$ -Al<sub>2</sub>O<sub>3</sub> ceramic substrate to the metallic Al droplet) to the metallic droplet because of the strong interaction between O and Al. The temperature of the diffused O atoms, which participated in chemical reactions, is initially higher than that of the solid ceramic substrate. Namely, the resulting increase in temperature increases reactivity, leading to the ready penetration

of O ions into the metallic Al droplet and consequently significant interfacial structural changes. Notably, when the metallic Al droplet wets the  $\alpha$ -Al<sub>2</sub>O<sub>3</sub> substrate, the Al atoms in the droplet do not penetrate into the  $\alpha$ -Al<sub>2</sub>O<sub>3</sub> substrate.

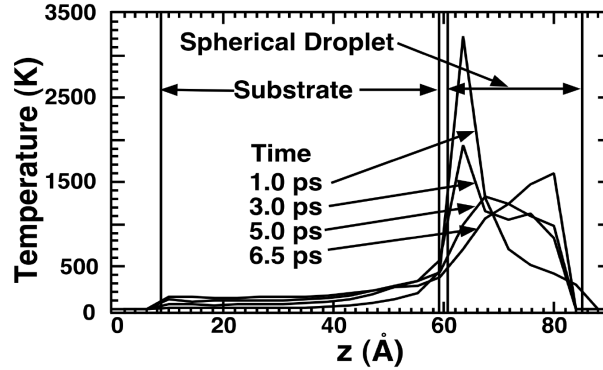


**Figure 4.** Time evolution of the temperature profile along the  $z$ -direction during the reactive wetting of the  $\alpha$ -Al<sub>2</sub>O<sub>3</sub> substrate by the spherical Al droplet, shown at  $t = 1.0, 3.0, 5.0,$  and  $6.5$  ps. The vertical lines mark the top and bottom of the initial substrate and the droplet.

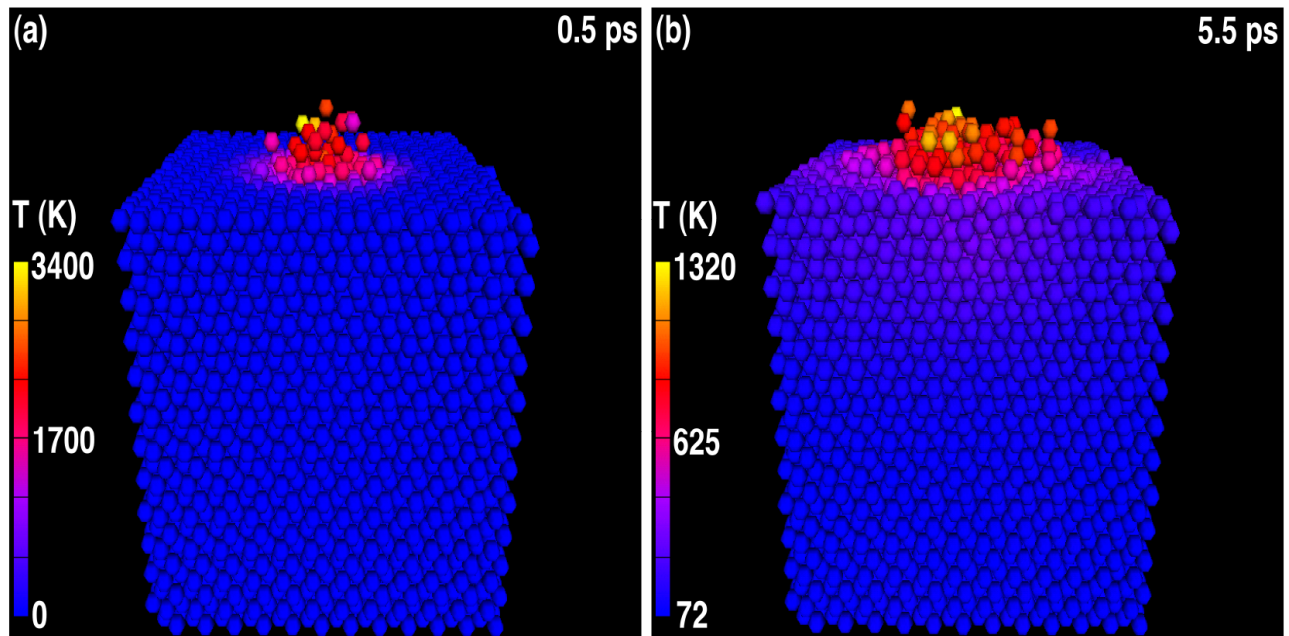


**Figure 5.** Snapshots of the temperature of oxygen atoms at times of (a) 0.5 ps and (b) 5.5 ps during the wetting of the solid ceramic by the metallic Al spherical droplet. The spheres are O atoms (Al atoms are removed for clear representation) and color represents the temperature of an atom.

Figure 6 shows the number density profile for O atoms along the  $z$ -direction at time  $t = 8.5$  ps, calculated with bins of size 1.3 Å. In the beginning, the topmost O layer of the ceramic substrate is placed at  $z$  of  $\sim 5.92$  nm. At the end of the wetting process ( $t = 8.5$  ps), the O number density above  $z$  of  $\sim 50$  Å (which corresponds to the topmost  $\sim 5$  oxygen layers) is reduced from the initial value in the ceramic substrate. This indicates the

mass transport of oxygen atoms within 1.0 nm from the interface into the Al droplet, where they contribute to the wetting by participating in the chemical bonding and forming a continuous oxide layer. The topmost location of the diffused O atoms from the ceramic surface to the spherical metallic droplet is  $z = 6.65$  nm.

We also study the temporal evolution of the contact angle between the metallic droplet and the ceramic substrate. The average contact angle of the droplet is calculated directly from a snapshot of the metallic droplet as the average,  $\theta = (\theta_{left} + \theta_{right})/2$  (see Figure 7), with the error bar,  $\Delta\theta = |\theta_{left} - \theta_{right}|/2$ . Figure 8 shows the time evolution of the average contact angle  $\theta$  for the spherical metallic Al droplet on the flat ceramic substrate. It significantly reduces from  $145^\circ$  to  $47^\circ$  with time. The heat transfer across the interface causes a temperature increase in the Al droplet and consequently enhances the mobility of the aluminum atoms. As a result, the metallic droplet spreads over the ceramic substrate and the contact angle decreases, with the sharpest decrease observed at  $t$  of  $\sim 1.6$  ps. A similar decrease of the contact angle has been observed experimentally [19], which can be understood as a decrease in the Al/ $\text{Al}_2\text{O}_3$  energy  $\gamma_{LS}$  in Young's equation, Equation (1), due to chemical reactions.

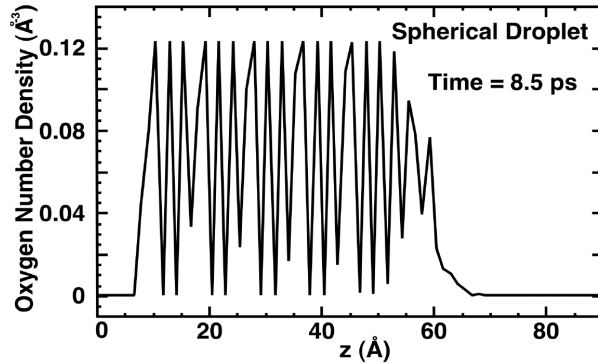


**Figure 6.** Oxygen number density distribution combined with diffusion of O atoms from ceramic substrate to droplet in the  $z$ -direction at end of wetting process,  $t = 8.5$  ps.

The present results are consistent with previous computational and experimental studies of the wetting process. For example, recently, Tigli et al. employed ReaxFF reactive MD simulations to investigate the wetting processes in an Al and alumina system [34]. They revealed that some of the oxygen atoms diffused into the molten Al droplet within a range of  $10 \text{ \AA}$ , which indicated that the solubility limit of oxygen in liquid Al droplets was very limited. They further noted that diffusion of oxygen atoms was more likely to be responsible for the formation of the new layer at the triple junction along the Al/alumina interface, similarly to the present results. Additionally, they reported that contact angles of the Al droplet on the alumina substrate increased with droplet size at the same temperatures. For example, contact angles were  $68^\circ$ ,  $77^\circ$ ,  $96^\circ$ , and  $111^\circ$  and the size of the droplet was 16, 24, 32, and  $40 \text{ \AA}$  at 700 K, respectively. Shen et al. highlighted the effect of the preexistence of the oxide shell layer on the liquid Al droplet on wettability, including the dissolution and the contact angle, during the wetting process between liquid Al and an  $\text{Al}_2\text{O}_3$  substrate [35]. They reported that the final stable contact angle was approximately  $63^\circ$  above  $1275^\circ \text{C}$  under vacuum conditions. Komolafe et al. indicated that interfacial chemical reactions between the liquid drop and substrate at the interface were accompanied by the form of dissolution, intermetallic formation, or a combination of both processes including microstructural changes in any reactive system during the wetting process [36]. Lee et al. studied the wetting behavior at the liquid Al/solid  $\alpha\text{-Al}_2\text{O}_3$  interface [37]. They found that the oxygen-induced structural changes



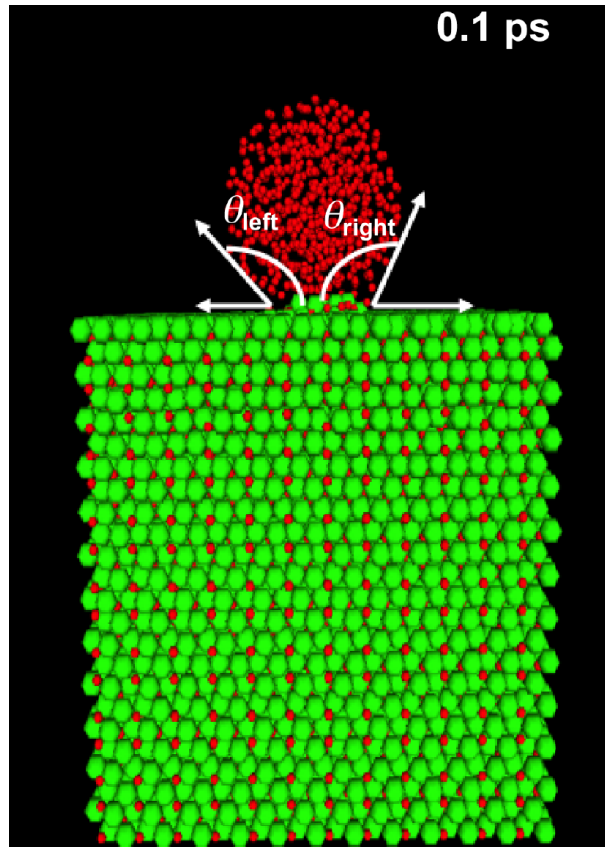


**Figure 7.** A side view of the spherical Al droplet on the  $\alpha\text{-Al}_2\text{O}_3$  substrate at time 0.1 ps, showing the contact angles,  $\theta_{left}$  and  $\theta_{right}$ .

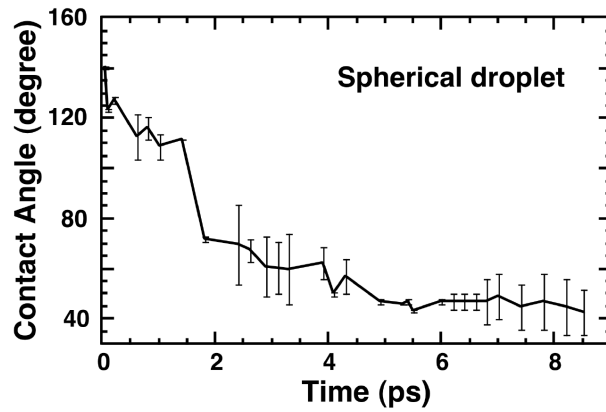


**Figure 8.** Time evolution of the wetting contact angle between the spherical metallic droplet and the flat ceramic substrate.

at the interface occurred within the first few liquid layers, leading to the wetting of liquid Al on the solid  $\alpha\text{-Al}_2\text{O}_3$ .

The diffusion of oxygen atoms and the resulting lower oxygen number density in the reactive region (see Figure 6) suggest that the structure of the substrate near the spherical Al droplet differs from that of the bulk  $\alpha$ -alumina. We study local structural correlations in the reactive region by calculating the radial distribution

function (RDF) for Al-O atomic pairs, the average atomic coordination number for Al-O atomic pairs, and bond angle distributions for Al-O-Al and O-Al-O atoms. We have calculated the RDFs of Al-O atomic pairs in the region,  $z = 5.0\text{--}7.0$  nm, which match the chemically reactive region, as shown in Figure 9. The Al-O RDFs show first and second characteristic peaks at 1.83 and 3.55 Å, respectively. As a comparison, the first-neighbor distances in the  $\alpha$ -alumina crystal are 1.86 and 1.96 Å [27].

The average coordination number for Al atoms, computed by integrating the Al-O RDFs up to  $r = 2.7$  Å, is 5.5 in the region of  $z = 5.0\text{--}7.0$  nm, whereas it is 6 (which is the same as the  $\alpha\text{-Al}_2\text{O}_3$  crystal's value) at  $z = 5.0\text{--}6.0$  nm and 2.6 at  $z = 6.0\text{--}7.0$  nm. The Al coordination number thus decreases along the  $z$ -direction, where the density of oxygen atoms decreases. The corresponding angular distributions for Al-O-Al and O-Al-O, calculated with the Al-O cutoff distance of 2.5 Å, are clearly shown in Figure 10 at  $t = 8.5$  ps. The bond angle distribution for Al-O-Al shows that distinct peaks are located at  $\sim 87^\circ$ ,  $120^\circ$ , and  $136^\circ$ . On the other hand, first sharp peaks at  $87^\circ$  and second peaks at  $162^\circ$  were observed for the O-Al-O bond angle distribution. For comparison, the Al-O-Al bond angles in crystalline  $\alpha\text{-Al}_2\text{O}_3$  ceramic are  $84.76^\circ$ ,  $93.61^\circ$ ,  $120.38^\circ$ , and  $132.19^\circ$  and those for O-Al-O are  $79.53^\circ$ ,  $86.4^\circ$ ,  $101.2^\circ$ , and  $164.13^\circ$ [38].

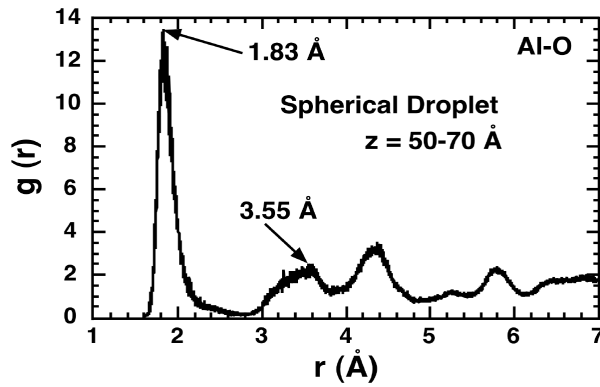


**Figure 9.** Radial pair-distribution function of Al-O interactions in the region of  $z = 5.0\text{--}7.0$  nm at end of the wetting process. The arrows show the first- and second-neighbor distances in the crystalline  $\alpha\text{-Al}_2\text{O}_3$ .

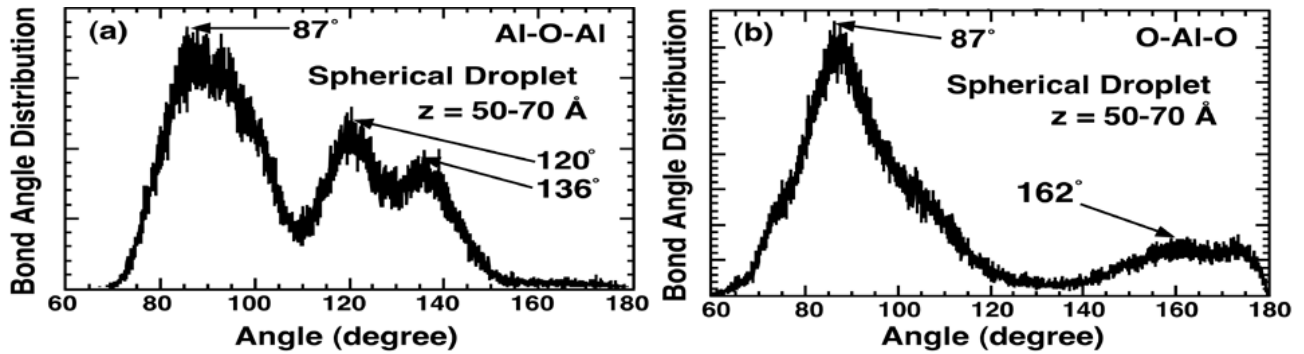
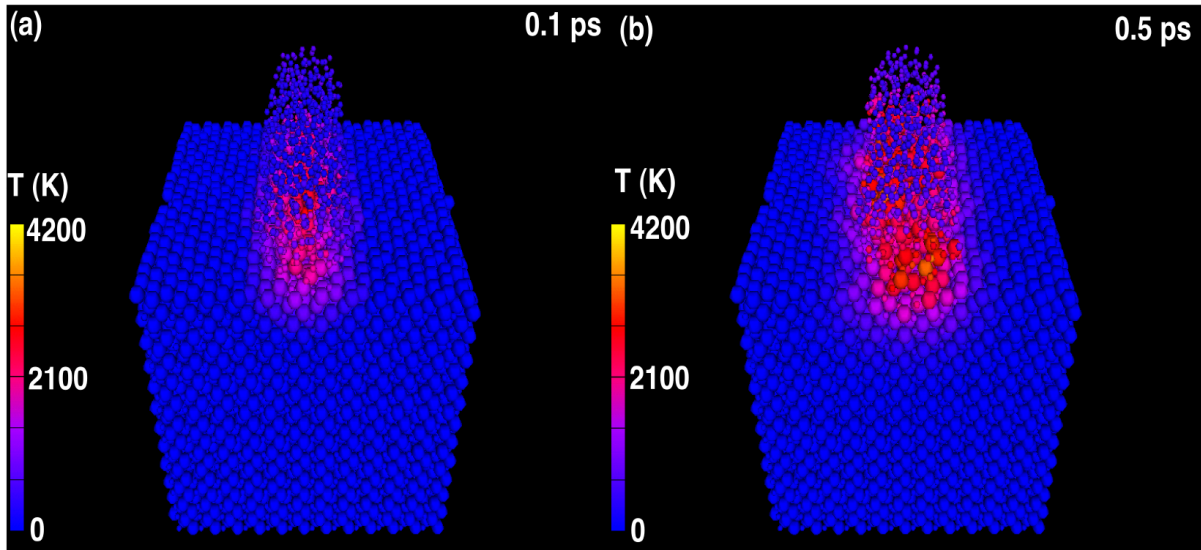


**Figure 10.** Bond-angle distributions function of (a) Al-O-Al and (b) O-Al-O in the region of  $z = 5.0\text{--}7.0$  nm at the end of the wetting process. The arrows show the Al-O-Al and O-Al-O angles in the crystalline  $\alpha\text{-Al}_2\text{O}_3$ .

### 3.2. Effects of droplet shape: results for cylindrical and layer nanodroplets

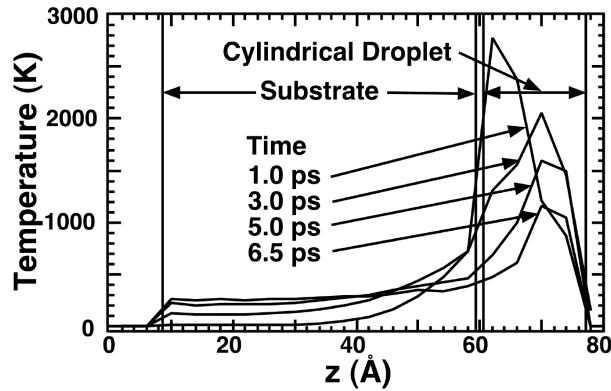
In addition to the spherical shape, we have simulated two additional shapes (cylindrical and layer) for the Al droplet. The cylindrical and layer Al droplets are placed on the same substrate as used in the spherical Al droplet simulations. The length of the cylinder Al droplet, which is parallel to the y-axis, is 5.75 nm. Figure 11 shows the temperature distribution in the cylindrical droplet simulation at  $t = 0.1$  and  $0.5$  ps. We again observe the release of heat in the reactive region, where the cylindrical Al droplet contacts the flat  $\alpha$ -Al<sub>2</sub>O<sub>3</sub> substrate.

Figure 12 shows the temperature distribution with the temperature propagation profile along the z-direction for the sample cylindrical metallic droplet. Similarly to the case of the spherical droplet, the wetting of the  $\alpha$ -Al<sub>2</sub>O<sub>3</sub> substrate by the Al droplet is accompanied by chemical reactions between Al and O atoms in the reactive interface. In the case of the cylindrical droplet, the contact area of the droplet/ceramic interface and hence the number of atoms participating in the chemical reactions are larger than those in the spherical droplet case. This leads to higher rates of heat production and a move from the contact area to the ceramic and the metallic droplet. Consequently, the ceramic substrate temperature for the cylindrical metallic droplet ( $\sim 190$  K at 3 ps; see Figure 12) is higher than that ( $\sim 89$  K at 3 ps) in the spherical metallic droplet case.



**Figure 11.** The temperature distribution of atoms within contact regions at the ceramic/metallic droplet interface at (a) 0.1 ps and (b) 0.5 ps during the wetting process. Actual temperature distribution in the contact region suddenly increases to  $\sim 4200$  K. The larger and smaller spheres show O and Al atoms, respectively. The colors denote the temperature of atoms.

Figure 13 shows the time evolution of the temperature profile along the z-direction in the layer Al droplet case, which corresponds to complete wetting. The number of atoms participating in chemical reactions for the layer droplet case is larger than that in the spherical and cylindrical droplet cases, and as a result, chemical reactions initially produce much larger heat. This is quantified by calculating the average temperature of atoms at  $t = 3$  ps, which is 162 K, 298 K, and 381 K for the spherical, cylindrical, and layer droplet cases, respectively. At  $t = 0.5$  ps, the temperature at the contact region of the interface rises to 3300 K, which is higher than the melting temperatures of metallic Al (930 K) and ceramic  $\alpha$ -Al<sub>2</sub>O<sub>3</sub> (2053 K). The higher rates of heat production and transfer are also reflected by the broader distributions of the temperature. For example,



**Figure 12.** Time evolution of the temperature profile along the  $z$ -direction for the cylindrical Al droplet on the  $\text{Al}_2\text{O}_3$  substrate. The vertical lines mark the top and bottom of the initial substrate and droplet.

the full-width at half-maximum of the highest temperature peak in the temperature profile at  $t = 1$  ps is 6 Å, 11 Å, and 17.5 Å for spherical, cylindrical, and layer droplet cases, respectively.

Structural local correlations near the interface are also analyzed for the metallic layer Al droplet case, allowing characterization of the bonding, microstructure, and chemistry of the interface upon the resulting wetting process. The results of RDFs for the Al-O pair in the region,  $z = 5.0\text{--}7.0$  nm, is shown in Figure 14. The position of the first distinct peak is 1.81 Å, which is slightly smaller than that in the spherical droplet case (1.83 Å). The corresponding coordination number for Al is 3.4 in the region of  $z = 50\text{--}70$  Å. The Al atoms are surrounded by 5 and 1.6 O atoms in the regions of  $z = 5.0\text{--}6.0$  nm and  $z = 6.0\text{--}7.0$  nm, respectively, which corresponds to the average coordination numbers. The average coordination number of Al reduces for larger  $z$ , where O density decreases.

Figure 15 corresponds to the Al-O-Al and O-Al-O bond angle distributions in the region,  $z = 5.0\text{--}7.0$  nm, for the layer metallic droplet at time  $t = 6.5$  ps. There are two sharp peaks in the Al-O-Al bond angle distribution at  $90^\circ$  and  $137^\circ$ ; see Figure 15a. These values differ substantially from those in the spherical Al droplet case. The O-Al-O bond angle distribution in Figure 15b has two sharp peaks at  $89^\circ$  and  $110^\circ$ . As compared with the spherical Al droplet case ( $87^\circ$ ), this peak is shifted toward a larger angle.

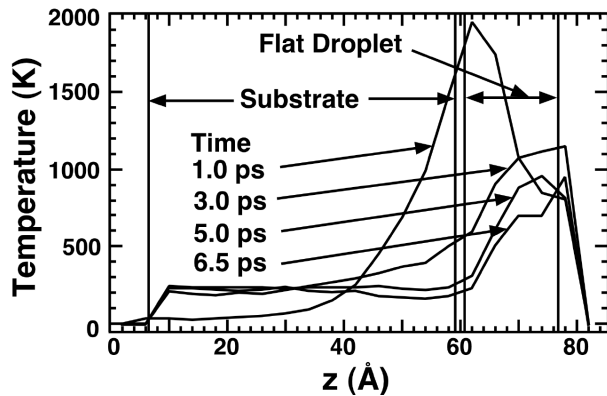


**Figure 13.** Time evolution of the temperature profile along the  $z$ -direction for the layer Al droplet on the  $\text{Al}_2\text{O}_3$  substrate. The vertical lines mark the top and bottom of the initial substrate and droplet.

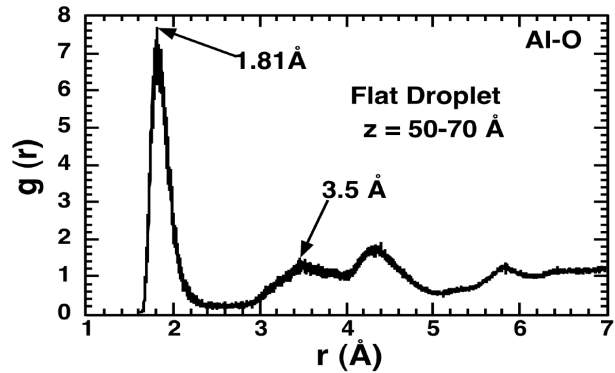


**Figure 14.** The Al-O pair distribution function in the region at  $t = 6.5$  ps for the layer metallic droplet case.

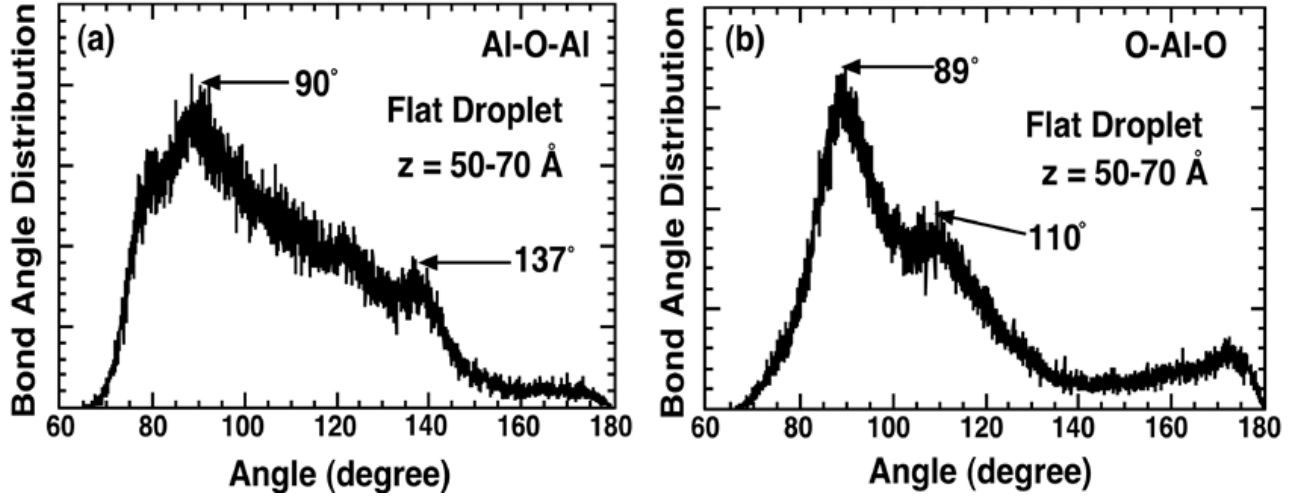


Figure 15. Angle distributions for (a) Al-O-Al and (b) O-Al-O of the layer metallic droplet case at  $t = 6.5 \text{ ps}$ .

#### 4. Conclusions

We have performed variable-charge MD simulations on parallel computers to study the reactive wetting of a flat  $\alpha\text{-Al}_2\text{O}_3$  ceramic substrate by a metallic Al droplet for three different initial shapes of the droplet: spherical, cylindrical, and layer. Our simulation results show that the chemical reactions create intensive heat around the contact region at the interface. Consequently, it is transferred from the reactive site to the solid ceramic substrate and metallic droplet, which causes solid-to-liquid transitions in the Al droplet and  $\alpha\text{-Al}_2\text{O}_3$  substrate near the reactive region. As a result of the heat transfer, the Al droplet partially spreads over the flat  $\alpha\text{-Al}_2\text{O}_3$  substrate. Diffusion of oxygen atoms into the Al droplet, resulting from the dissolution of the ceramic, causes the formation of a continuous and oxygen-rich reaction product layer and changes the structure of the interface. Significant atomic charge transfer between Al and O atoms is observed in this reactive region, which results in the formation of strong ionic bonding and contributes to the adhesion of the Al/ $\alpha\text{-Al}_2\text{O}_3$  interface. The reaction product at the interface is chemically stable, and accordingly, further reaction between the droplet and substrate decreases with time and eventually terminates. The increased physical contact area between the Al droplet and the  $\alpha\text{-Al}_2\text{O}_3$  substrate, from spherical to cylindrical to layer shape, results in increased numbers of atoms participating in the chemical reaction at the interface and thus causes enhanced heat production.

The present simulation has studied reactive wetting in a vacuum. However, aluminum is known to readily oxidize in air to form stable oxide layers on the surface, due to its extremely high oxygen affinity. (We have performed variable-charge MD simulations of the oxidation of an Al nanoparticle [26].) The oxidation layer on the liquid aluminum is one of the critical factors to affect the reactive-wetting kinetics and wettability [7,18,24]. Clearly, the oxidation of Al surfaces reduces the reactivity between the ceramic substrate and the Al liquid metal, and alters the measured value of the contact angle. To avoid this problem, experimental studies of Al/ $\alpha\text{-Al}_2\text{O}_3$  systems are usually performed under conditions that inhibit the initial oxide layer's formation [24]. Wang et al. [39] showed that oxygen contamination at the liquid/solid interface affects the wettability; the contact angle of an aluminum droplet on sapphire was  $90^\circ$  without the oxygen contamination, and it was  $\sim 105^\circ$  when contamination was present. We are currently planning MD simulations to study the wetting of an  $\alpha\text{-Al}_2\text{O}_3$  substrate by an Al droplet in oxygen environment.

## Acknowledgment

The author would like to thank Prof. Dr. Priya Vashishta and Prof. Dr. Aiichiro Nakano for their comments and discussions in the preparation of the manuscript.

## References

- [1] Aksay IA, Hoye CE, Pask JA. Wetting under chemical equilibrium and non-equilibrium conditions. *Journal of Physical Chemistry* 1974; 78 (12): 1178-1183. doi: 10.1021/j100605a009
- [2] Howe JM. Bonding, structure, and properties of metal/ceramic interfaces: part 1 chemical bonding, chemical reaction, and interfacial structure. *International Materials Reviews* 1993; 38 (5): 233-256. doi: 10.1179/imr.1993.38.5.233
- [3] Eustathopoulos N. Dynamics of wetting in reactive metal/ ceramic systems. *Acta Materialia* 1998; 46 (7): 2319-2327. doi: 10.1016/S1359-6454(98)80013-X
- [4] Chidambaram PR, Edwards GR, Olson DL. A thermodynamic criterion to predict wettability at metal-alumina interfaces. *Metallurgical Transactions B* 1992; 222: 215-222. doi: 10.1007/BF02651856
- [5] Tomsia AP, Saiz E, Foppiano S, Cannon RM. Proceedings of the 2nd International Conference on High Temperature Capillarity, Krakow, Poland, 29 June–2 July 1997. Krakow, Poland: Foundry Research Institute, 1998.
- [6] Chen J, Gu M, Pan F. Reactive wetting of a metal/ceramic system. *Journal of Materials Research* 2002; 17 (4): 911-917. doi: 10.1557/JMR.2002.0133
- [7] Feng YB, Zhang X, Yang B, Yang BM, Chen Z. Reactions and microstructures evolution in Al<sub>2</sub>O<sub>3</sub>-Al system in vacuum. *Asia-Pacific Journal of Chemical Engineering* 2018; 13 (1): 1-10. doi : 10.1002/apj.2144
- [8] Pilania G, Thijsse BJ, Hoagland RG, Lazic I, Valone SM et al. Revisiting the Al/Al<sub>2</sub>O<sub>3</sub> interface: coherent interfaces and misfit accommodation. *Scientific Reports* 2014; 4: 1-9. doi: 10.1038/srep04485
- [9] Zeng HD, Cheng XL, Zhang CY, Lu ZP. Responses of core-shell Al/Al<sub>2</sub>O<sub>3</sub> nanoparticles to heating: ReaxFF molecular dynamics simulations. *Journal of Physical Chemistry C* 2018; 122 (16): 9191-9197. doi: 10.1021/acs.jpcc.8b01088
- [10] Torrisi L, Scolaro C. Treatment techniques on aluminum to modify the surface wetting properties. *Acta Physica Polonica A* 2015; 128: 48-53. doi: 10.12693/APhysPolA.128.48
- [11] Zhang P, Fang J, Fu R, Gu X, Fei M. Bonding of Al to Al<sub>2</sub>O<sub>3</sub> via Al-Cu eutectic method. *Materials and Design* 2015; 87: 619-624. doi: 10.1016/j.matdes.2015.08.065
- [12] Sobczak N, Asthana R, Radziwill W, Nowak R, Kudyba A. The role of aluminum oxidation in the wetting-bonding relationship of Al/oxide couples. *Archives of Metallurgy and Materials* 2007; 52: 55-65.
- [13] Bao S, Tang K, Kvithyld A, Tangstad M, Engh TA. Wettability of aluminum on alumina. *Metallurgical and Materials Transactions B* 2011; 42: 1358-1366. doi: 10.1007/s11663-011-9544-z.
- [14] Oh SY, Cornie JA, Russell KC. Wetting of ceramic particulates with liquid aluminum alloys: Part II. Study of wettability. *Metallurgical Transactions A* 1989; 20 (3): 533-541. doi: 10.1007/BF02653933
- [15] George L, Kaplan WD. Oxygen induced interfacial phenomena during wetting of alumina by liquid aluminium. *Acta Materialia* 2002; 50 (1): 75-88. doi: 10.1016/S1359-6454(01)00333-0
- [16] de Gennes PG. Wetting: statics and dynamics. *Review of Modern Physics* 1985; 57 (3): 827-863. doi : 10.1103/RevModPhys.57.827
- [17] Landau LD, Lifshitz EM. *Statistical Physics*. 3rd. ed. New York, NY, USA: Pergamon Press, 1989.
- [18] Laurent V, Chatain D, Chatillon C, Eustathopoulos N. Wettability of mono crystalline alumina by aluminium between its melting point and 1273 K. *Acta Metallurgica* 1988; 36 (7): 1797-1803. doi : 10.1016/0001-6160(88)90248-9
- [19] Carnahan RD, Johnston TL, Li CH. Some observations on the wetting of Al<sub>2</sub>O<sub>3</sub> by aluminum. *Journal of the American Ceramic Society* 1958; 41 (9): 343-347. doi: 10.1111/j.1151-2916.1958.tb12931.x
- [20] Swiler TP, Loehman RE. Molecular dynamics simulations of reactive wetting in metal-ceramic systems. *Acta Materialia* 2000; 48: 4419-4424. doi: 10.1016/S1359-6454(00)00228-7

- [21] Ruhle M, Evans AG. Structure and chemistry of metal/ceramic interfaces. *Materials Science and Engineering A* 1989; 107: 187-197. doi: 10.1016/0921-5093(89)90387-0
- [22] Vasiliev I, Chelikowsky JR, Martin RM. Surface oxidation effects on the optical properties of silicon nanocrystals. *Physical Review B* 2002; 65 (12): 121302-12109. doi: 10.1103/PhysRevB.65.121302
- [23] Streit FH, Mintmire JW. Electrostatic potentials for metal-oxide surfaces and interfaces. *Physical Review B* 1994; 50 (16): 11996-12003. doi: 10.1103/PhysRevB.50.11996
- [24] Brenner DW. The art and science of an analytic potential. *Physica Status Solidi B* 2000; 217: 23-40. doi: 10.1002/(SICI)1521-3951(200001)217:1<23::AID-PSSB23>3.0.CO;2-N
- [25] Bazant MZ, Kaxiras E, Justo JF. Environment-dependent interatomic potential for bulk silicon. *Physical Review B* 1997; 56 (14): 8542-8552. doi: 10.1103/PhysRevB.56.8542
- [26] Campbell T, Kalia RK, Nakano A, Vashishta P. Dynamics of oxidation of aluminum nanoclusters using variable charge molecular dynamics simulations on parallel computers. *Physical Review Letters* 1999; 82 (24): 4866-4869. doi: 10.1103/PhysRevLett.82.4866
- [27] Iczkowski RP, Margrave JL. Electronegativity. *Journal of the American Chemical Society* 1961; 83 (17): 3547-3551. doi: 10.1021/ja01478a001
- [28] Rappe AK, Goddard WA. Charge equilibration for molecular dynamics simulations. *Journal of Physical Chemistry* 1991; 95 (8): 3358-3363. doi: 10.1021/j100161a070
- [29] Nakano A, Kalia RK, Vashishta P. Scalable molecular-dynamics, visualization, and data management algorithms for materials simulations. *IEEE Computing in Science and Engineering* 1999; 1 (5): 39-47. doi: 10.1109/5992.790586
- [30] Dorre E, Hubner H. *Alumina Processing, Properties, and Applications*. New York, NY, USA: Springer-Verlag, 1984.
- [31] Allen MP, Tildesley DJ. *Computer Simulation of Liquids*. New York, NY, USA: Oxford University Press, 1987.
- [32] Vashishta P, Kalia RJ, Nakano A, Li W, Ebbsjo I. *Amorphous Insulator and Semiconductors*. Amsterdam, the Netherlands: Kluwer Academic Publishers, 1997.
- [33] Minkowycz WJ, Sparrow EM. *Advances in Numerical Heat Transfer*. New York, NY, USA: Taylor & Francis, 2000.
- [34] Tigli A, Cagin T. A case study on metal-ceramic interfaces: wetting of alumina by molten aluminum. *Materials Science Forum* 2018; 915: 185-189. doi: 10.4028/www.scientific.net/MSF.915.185
- [35] Shen P, Zhang L, Wang Y. Influence of oxidation on contact angle between liquid aluminum and Al<sub>2</sub>O<sub>3</sub>. *Williams Eds Light Metals* 2016; 827-832. doi: 10.1007/978-3-319-48251-4\_140
- [36] Komolafe B, Medraj M. Progress in wettability study of reactive systems. *Journal of Metallurgy* 2014; 2014: 1-14. doi: 10.1155/2014/387046
- [37] Lee SB, Kim YM. Direct observation of in-plane ordering in the liquid at a liquid Al/ $\alpha$ -Al<sub>2</sub>O<sub>3</sub>(1102) interface. *Acta Materialia* 2011; 59: 1383-1388. doi: 10.1016/j.actamat.2010.10.069
- [38] Ishizawa N, Miyata T, Minato I, Marumo F, Iwai S. A structural investigation of  $\alpha$ -Al<sub>2</sub>O<sub>3</sub> at 2170 K. *Acta Crystallographica B* 1980; 36: 228-230. doi: 10.1107/S0567740880002981
- [39] Wang DJ, Wu ST. The influence of oxidation on the wettability of aluminum on sapphire. *Acta Metallurgica et Materialia* 1994; 42 (12): 4029-4034. doi: 10.1016/0956-7151(94)90180-5